Investigation of Pitting Corrosion in Sensitized Modified High-Nitrogen 316LN Steel After Neutron Irradiation

Citation: Merezhko, D. A., et al. "Investigation of Pitting Corrosion in Sensitized Modified High-Nitrogen 316LN Steel After Neutron Irradiation." Proceedings of the 18th International Conference on Environmental Degradation of Materials in Nuclear Power Systems – Water Reactors, 13-17 August, 2017, Portland, Oregaon, edited by John H Jackson et al., Springer International Publishing, 2018, pp. 1125–40.

As Published: http://dx.doi.org/10.1007/978-3-319-67244-1_71

Publisher: Springer International Publishing

Persistent URL: http://hdl.handle.net/1721.1/118600

Version: Author's final manuscript: final author's manuscript post peer review, without publisher's formatting or copy editing

INVESTIGATION OF PITTING CORROSION IN SENSITIZED MODIFIED HIGH-NITROGEN 316LN STEEL AFTER NEUTRON IRRADIATION

D. A. Merezhko[1], M. S. Merezhko[1], M. N. Gussev[2],
J. T. Busby[2], O. P. Maksimkin[1], M. P. Short[4], F. A. Garner[3]

[1] Institute of Nuclear Physics, Almaty, Kazakhstan, diana@inp.kz, 8(727) 386-6800
[2] Oak Ridge National Laboratory, Oak Ridge, TN 37831, USA, gussevmn@ornl.gov, (865) 574-4456
[3] Moscow Engineering Physics Institute, Russia; Radiation Effects Consulting, USA, frank.garner@dslextreme.com, 1-509-521-1633
[4] Department of Nuclear Science and Engineering, Massachusetts Institute of Technology, Cambridge, MA, 02139, USA, hereiam@mit.edu, (617) 347-7763

Formatted: Font: 10 pt, Font color: Black, English (United States)

Keywords: austenitic stainless steel, alloying, nitrogen, tungsten, copper, sensitization, pitting corrosion, grain boundary engineering

Abstract

The influence has been studied of thermo-mechanical treatment, sensitization conditions, and neutron irradiation on the pitting corrosion resistance of austenitic 316LN stainless steel variants in 10% $FeCl_3 \cdot 6H_2O$ at 22°C. Variants of this steel were modified with additions of nitrogen, manganese, copper, and tungsten, as well as testing cast, cold-rolled, grain boundary engineered (GBE), and as-received variants. It was found that the 316LN steel variant with additions of 0.2 % N and 2 % Mn had the best pitting corrosion resistance of all studied conditions. When irradiated in a light water reactor (LWR) to a maximum fluence of $3 \cdot 10^{17}$ n/cm^2 (E > 1.1 MeV, T_{irr} < 50°C), neutron irradiation surprisingly increased the resistance of GBE steels to pitting corrosion. An anisotropy of corrosion resistance of GBE and cold rolled steels was observed.

1. Introduction

Austenitic stainless steels are widely used in industry because of their excellent combination of mechanical properties and corrosion resistance. The latter is attributed to the thin passive oxide film that forms spontaneously on their surface in oxidizing environments, if the steel has a minimum chromium content of approximately 10.5 %. As a result, these steels are also chosen as suitable materials to construct internal components of nuclear reactors. However, the corrosion resistance of austenitic steels may decrease after aging at a temperature range of 550 - 800°C [1, 2]. In this temperature range, carbon diffuses toward the grain boundaries and forms chromium-rich carbides, producing Cr-depleted areas on the boundary between the carbides. The normal passivation reaction is thereby limited in these Cr-depleted regions, and the steel becomes susceptible to intergranular corrosion.

Pitting corrosion is an important and especially damaging type of localized corrosion. There is strong correlation between water quality and corrosion of fuel assemblies by pitting [3]. The resistance to pitting depends on both the material susceptibility and the environmental conditions. These include the chemical composition, heat treatment, grain size, sensitization, and other metallurgical parameters [4, 5] of the steel, as well as the presence of halogen anions [REF], radiolytic species such as peroxides [REF], and the pH of the surrounding water [REF]. Initiation and growth of corrosion pits are usually observed as a consequence of compositional heterogeneity and/or structural imperfections, especially associated with non-metallic inclusions or surface roughness [6]. Thus, many inhomogeneities, whether naturally present in the material or induced due to fretting, foreign material abrasion, or oxide rupture [REF], can nucleate corrosion pits to form.

One of the ways to enhance pitting resistance is by alloying with specific elements. It has been shown that nitrogen doping (sometimes with the addition of manganese) leads to improved corrosion resistance and mechanical performance [7-9]. Nitrogen doping also increases the strength level [10], improves deformation hardening behavior, and increases austenite stability during cooling and plastic deformation [11, 12]. The addition of copper also stabilizes austenite [13], improves alloy deformability, and increases the general corrosion resistance of stainless steels in sulphuric media [14]. There are a lot of available data about the localized corrosion in steels alloyed with copper [15-19], but there is no generally accepted overall view on the single-effect influence of the copper on corrosion behavior, particularly on pitting and crevice corrosion. The effects of other elements, such as manganese, molybdenum, silicon, aluminum, and some others, on mechanical properties have been widely investigated [20-22].

It is of particular interest to study the corrosion resistance of large components or complex shapes as a function of processing. Particularly noteworthy examples include shield modules or divertors for ITER [23], or LWR internals such as ___ [FRANK – what is the funny shaped bottom plate called that holds the fuel assembles?]. While casting such large, complex parts can simplify their production and reduce their price [24], this often comes with a decrease in strength compared to forged parts. Mechanical properties of cast materials can also exhibit much local variation, due to the larger grain size of ingots, lower dislocation densities, and extensive segregation of alloying elements and impurities during the solidification process [REF]. Alloying with nitrogen and copper makes it possible to produce cast steels with generally more favorable mechanical properties and corrosion resistance [25].

For many austenitic steels, grain boundary engineering (GBE) may provide a way to increase resistance to stress corrosion cracking and pitting corrosion and improve the resistance to sensitization [28-30]. GBE consists of a set of thermo-mechanical treatments to encourage the formation of certain types of grain boundaries, often low-angle ones, which exhibit more resistance to sensitization and intergranular corrosion. It has been shown that specific low-energy grain boundaries, such as coincidence site lattice boundaries (often called Σ3, Σ9, or Σ27 grain boundaries) possess good resistance to carbide precipitation [26, 27].

The main goals of this work are to investigate the influence of neutron irradiation and sensitization on the corrosion resistance of compositional variants of austenitic AISI 316LN stainless steel in the cast and cold-rolled conditions. A particular focus is given to the effect of copper alloying content, as well as the effect of GBE on the resistance of these 316LN variants to pitting corrosion. This is therefore an exploratory study, seeking to determine optimum alloying additions and thermo-mechanical treatments to minimize the susceptibility of 316LN stainless steel to pitting corrosion.

2. Materials and methods of investigation

Formatted: English (United States)

2.1 Alloying

A reference material (30% cold-rolled 316LN) [31], supplied as an annealed bar with an average grain size of 50 μm, was used to provide baseline information about microstructure and corrosion resistance. Steel variants with modified compositions, designated as alloys 211 L though 213 L, were cast by Stainless Foundry and Engineering, Inc. using air induction melting with an argon cover gas. Materials with modified compositions were cast as small heats (100-150 pounds each). The elemental composition and calculated chromium and nickel equivalents [32] of the studied materials are shown in Table 1. Calculation of chromium and nickel equivalents showed that the investigated alloys are austenitic, completely stable against martensitic transformation.

Table 1: Chemical compositions of reference and modified steels (wt. %)*

Alloy	Cr	Ni	Mn	Si	Mo	C	N	Cu	W	Cr_{eq}	Ni_{eq}
316LN	17.5	12.5	1.8	0.50	2.5	0.03	0.07	0.30	–	22.25	16.14
211 L	17.7	12.5	4.1	0.44	2.5	0.02	0.34	0.31	–	22.33	23.74
212 L	17.7	12.6	5.1	0.44	2.5	0.01	0.36	2.8	–	22.33	25.29
213 L	17.7	12.6	5.1	0.45	2.0	0.01	0.32	2.8	1	22.35	24.29

*In all steels, S<0.01, P<0.03.

Alloy 211 L was designed with an increased amount of N and Mn. As noted above, N is a powerful solid solution strengthener. According to the literature, an increase of 0.1 wt. % N may increase the yield strength by up to 50 MPa [33]. The Mn content was increased to enhance the solubility of N, to reduce radiation-induced segregation of chromium, and to provide increased fluidity during casting. Increasing N and Mn would also be expected to also increase the stability of austenite. **Alloy 212 L** was designed with a further increase of Mn and an addition of Cu. The Mn content was increased to further enhance the stability of austenite. The addition of Cu was expected to improve the ductility and corrosion resistance, in addition to stabilizing austenite during casting and solidification. **Alloy 213 L** had an addition of W and an adjustment of Mo above that of 212 L. Tungsten was added to 213 L to improve resistance to localized corrosion even in sensitized steel [34], and to help to form a protective oxide film [35]. The combination of Mo and W will synergistically increase strength, and may also help improve pitting corrosion resistance.

2.2 Fabrication

After alloying, investigated materials were in the form of as-cast, 40 mm thick blocks. The fabrication process of each of the cold-rolled and GBE-steels is shown in Figure 1.

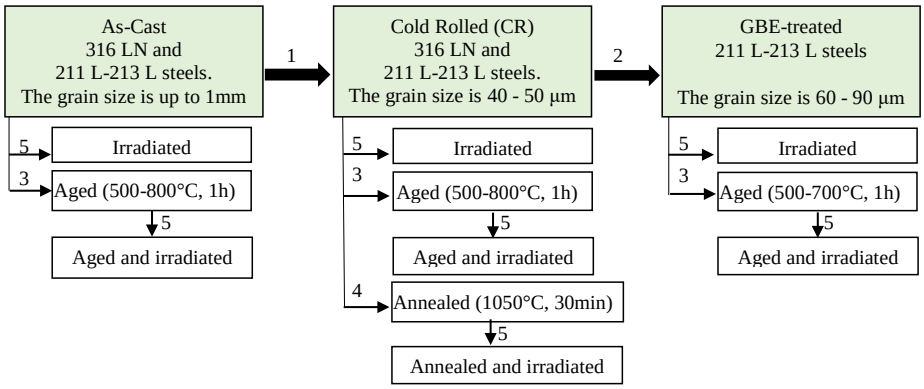

Figure 1: Fabrication methodologies of materials investigated in this study. All blocks represent thermo-mechanical states of materials investigated in this paper. Numbers correspond to processes of fabrication, with full descriptions in the text.

Each stage number in Figure 1 corresponds to one of the following treatments.

Treatment 1 produced cold-rolled steel with a regular grain size distribution, as a starting condition. As-cast blocks were subjected to a grain refinement procedure by hot-rolling followed by cold-rolling. After annealing at 1200°C in argon for one hour, 15 passes of hot-rolling were made with a 10-minute reheat between passes. Each pass reduced the thickness by about 2 mm, producing a final thickness of 10 mm. Then cold-rolling was conducted, further reducing the thickness from 10 mm to 7 mm. In cold-rolled materials, the fraction of special grain boundaries was measured to be 40 - 45 %.

Treatment 2 was the preparatory stage for obtaining a more fully GBE structure. This included the annealing of the cold-rolled plates and subsequent cooling in air by ~5°C/s. After annealing at 1050°C for 30 minutes, small plates of the modified steels were further rolled to a 5 % thickness reduction, and then annealed at 1050°C for two hours to reach a higher density of special grain boundaries (Figure 2b). The fraction of special grain boundaries was measured to be 75 - 80 % in these GBE-treated steels.

Treatment 3 consisted of an intentional sensitization treatment, to investigate the effect of sensitization of these steels on pitting corrosion. Specimens of cast, cold-rolled, and GBE steels were subjected to aging in the range of 500 - 800°C in a vacuum-filled tube for one hour, in order to encourage the precipitation of carbides at the grain boundaries. Afterwards, the specimens were quenched in room temperature water while still under vacuum. The temperature and time of aging was chosen to simulate the process of welding without proper post-weld heat treatment, as short-term heating to 500 - 800 °C can occur in the heat-affected zone during welding. In addition, similar temperatures can occur in the core of a nuclear reactor in accident conditions.

Treatment 4 represented a normalization treatment, performed to alleviate the effects of sensitization and dissolve the carbides formed in Treatment 3. This represents a desensitization process. Cold-rolled specimens were annealed at 1050°C for 30 minutes in a vacuum-filled tube, and then quenched in room temperature water while still under vacuum.

Treatment 5 was an irradiation treatment in low temperature LWR water, designed to investigate the effects of irradiation on as-cast, as-rolled, GBE, sensitized, and desensitized steels. After heat treatment, specimens from each initial condition (cast, cold-rolled, GBE) were irradiated with neutrons at the WWR-K LWR in Almaty, Kazakhstan (a pool-type 6 MW thermal nuclear reactor, $T_{irr} < 50$°C) to a maximum fluence of $3 \cdot 10^{17}$ n/cm^2 with E > 1.1 MeV

and $4.5 \cdot 10^{18}$ n/cm^2 with E < 0.4 eV. The fluence was mainly limited by reactor availability. A relatively small number of studies are devoted to low-dose irradiation, despite the fact that similar doses can be observed in real reactors. For example, the maximum fluence at the vessel wall after 40 years of operation for the French 900 and 1300 MWJ power plants is about 7 and 4 to 10^{19} n/cm^2 respectively [36].

Commented [MPS1]: This is two orders of magnitude off from your chosen fluence. Why are you mentioning it here? It only serves to make your studies look different from real conditions.

2.3 Gravimetric tests

Pitting corrosion behavior was investigated using the standard test for pitting corrosion resistance defined in ASTM G 48-03, method A [37]. The corrosion medium was 10% ferric chloride solution ($FeCl_3 \cdot 6H_2O$). The test temperature was 22±2°C with times chosen as 5, 24, 48 and 72 hrs. Samples of AISI 316 LN, 211 L, 212 L, and 213 L stainless steel (5 x 7 x 3 mm) were first polished using 120-grit sandpaper. Before the experiment samples were weighed on a Kern-770 balance with a precision of 0.1 mg. At the end of the corrosion test the specimens were taken out, cleaned by running water, rinsed in distilled water, dried in air, and then weighed again at room temperature to determine their mass loss.

Commented [MPS2]: Is that really the standard, you stopped polishing at 120 grit? I would have expected a much better polish required for an accurate pitting corrosion test. 120 grit can leave scratches 10's of microns deep, much deeper than pits.

The corrosion rate, V_{corr} (mm/year), was calculated for each test from the following equation:

$$V_{corr} = \frac{8.76 * \Delta m}{S \tau \rho} \quad (1)$$

where $\Delta m = m_0 - m_i$ is the weight change in grams; S is the area in m^2, τ is the time of exposure in hours, and ρ is the density in g/cm^3. The density measurement was performed using hydrostatic weighing.

3. Experimental results and discussion

Formatted: English (United States)

3.1 Microstructural analysis

Commented [MPS3]: I think you will need to show microstructures of 211 L, 212 L, and 213 L in each of the three starting conditions for a more uniform comparison.

Formatted: English (United States)

Typical microstructures and electron backscatter diffraction (EBSD) maps of cold-rolled 211 L steel and 212 L GBE-treated steel are shown in Figure 2. EBSD analysis of structural parameters (average misorientation, grain reference orientation deviation) showed a fully recrystallized, annealed structure in both cases. Subsequent metallurgical analysis showed clean grain boundaries without any precipitates. All steels contained an insignificant amount of non-metallic inclusions with specific string-like structures (Figure 2a), probably related to inter-dendritic precipitation in the original as-cast structure. One of stringer inclusions was analyzed using TEM and exhibited a typical oxide composition (Mn/SiO_2). We believe that most of these inclusions are oxides, and it is unlikely that a significant number of MnS inclusions are present in the materials. For all steels investigated, the grain structures were uniform and no small grain clusters were observed. No retained ferrite was observed in either the parent or modified steels.

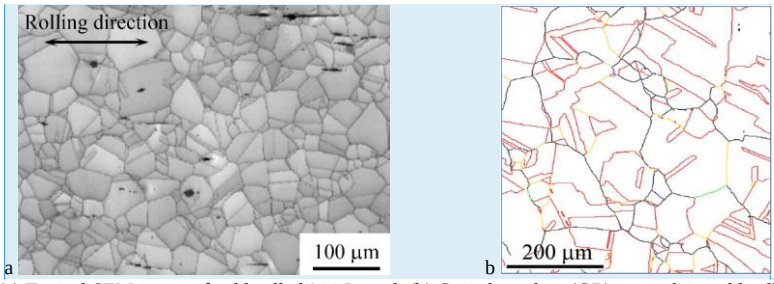

Figure 2: (a) Typical SEM image of cold-rolled 211 L steel. (b) Grain boundary (GB) network in cold-rolled 212 L steel after GBE. Black—random high-angle GBs, green—low-angle (<15°) GBs, red—Σ3 (twin) GBs, and yellow—Σ9, Σ27 GBs (high-order twins).

Commented [MPS4]: I think you should show an EBSD map for 211 L as well. Showing one SEM images for 211 L and one EBSD map for 212 L is confusing, the readers cannot make a direct comparison this way.

The microstructure of the as-cast 316 LN steel is shown in Figure 3a, while Figures 3b-c show the microstructures after cold-rolling and annealing, respectively. The cold-rolling has clearly broken up the dendritic, as-cast structure, while the normalization treatment (annealing) recrystallizes the material into a more typical austenitic, isotropic structure with little resemblance to either the cast or the rolled microstructures.

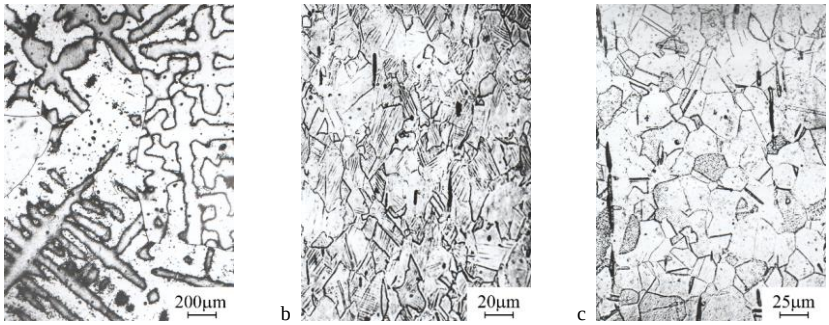

Figure 3: Microstructure of 316LN steel: dendritic structure in as-cast steel (a); deformation patterns in cold-rolled steel (b) and grain structure after annealing at 1050°C for 30min (c).

3.2 Mechanical properties

Table 2 shows averaged values of tensile strength σ_{uts}, yield strength σ_{02}, uniform elongation δ_u, and total elongation δ_{tot} for the specimens of cast, cold-rolled, and GBE-treated 211 L – 213 L steels tested at room temperature. Gauge section dimensions were of the SS-3 geometry (7.62×1.4×0.75 mm), and the strain rate was set at 0.5mm/min. It can be seen that the addition of nitrogen and manganese in all modified significantly increases the ultimate strength of cast material. Mechanical characteristics of GBE-treated 211L, 212L and 213L are not worse than those of the annealed AISI 316 LN [38]. In addition, the addition of copper appears to significantly increase the ductility of the as-cast steels, without sacrificing yield strength or ultimate tensile strength. This effect is absent in the cold-rolled and GBE variants. It is particularly noteworthy how much lower the yield stress of the GBE steels is compared to the cold-rolled condition, almost returning to the as-cast strength, along with much of the ductility. However, the increase in ultimate tensile strength is approximately 50% retained from the cold-rolling in the GBE condition.

Table 2: Mechanical characteristics of cast, cold rolled and GBE-treated 316 LN and 211-213 L steels

Condition	Material	σ_{02}, MPa	σ_{uts}, MPa	δ_u, %	δ_{tot}, %
Cast	AISI 316 LN	255	394	53	58,5
	211 L	255	488	52	59
	212 L	291	493	72,5	82
	213 L	241	467	59	67
Cold-Rolled	AISI 316 LN	800	835	4	22
	211 L	1030	1050	<1	11
	212 L	880	975	2.5	17
	213 L	930	1030	2	14
GBE	211 L	340	700	54,5	65
	212 L	345	745	47,5	58
	213 L	325	720	45	56,5

3.3 Effects of alloying and neutron irradiation on pitting corrosion resistance of 316 LN steel

The corrosion rates of irradiated 316 LN stainless steel and its variants alloyed by nitrogen, manganese, copper, and tungsten are shown in Figure 4. 316 LN steel in the as-cast condition exhibits good corrosion resistance in all irradiation conditions, which is probably due to its very large grain size. It was shown [39] that increasing the grain size of 316 LN stainless steel leads to less susceptibility to intergranular corrosion. The high-copper variants of 316LN (212 L and 213 L) show a markedly higher susceptibility to corrosion after neutron irradiation.

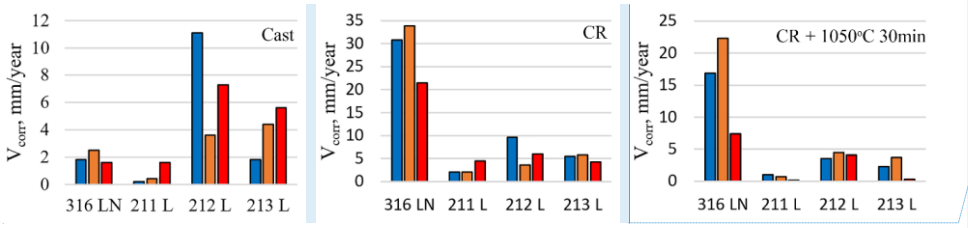

Figure 4: Corrosion rates of cast, cold-rolled (CR), and annealed cold-rolled (CR + 1050°C 30min) 316 LN stainless steel, unirradiated (blue), and irradiated by neutrons to $1x10^{17}$ n/cm^2 (orange) and $3x10^{17}$ n/cm^2 (red).

The cold-rolled initial 316LN material exhibits the highest susceptibility to corrosion in all irradiation conditions, as well as in the unirradiated form. The high internal stress level after cold-rolling is probably the cause of the observed decrease of corrosion resistance. Clear deformation patterns (Figure 3b) indicate a highly stressed state. According the literature [40] they appear in the grains loaded above the yield strength during the rolling of steels containing nitrogen. These deformation patterns occur not only because of deformation but also because of intensive etching caused by enrichment in nitride precipitates compared to that in non-deformed zones. All variants of the cold-rolled steel exhibit strikingly lower corrosion rates, both in the unirradiated and in the two irradiated conditions. In the case of 212 L, the corrosion resistance actually increases after irradiation, as it did in the as-cast condition.

After annealing at 1050°C for 30 min, the solubility of nitrogen increases, and stresses in the deformed grains are removed, such that the deformation patterns disappear (see Figure 3c) and the corrosion rate subsequently decreases in the unirradiated condition. Once again, the corrosion rates of all three compositional variants are 4-10x lower, with the 211 L exhibiting the lowest corrosion rate in nearly all cases.

Changes in material composition clearly lead to changes in corrosion behavior. The best pitting resistance is observed in the 211 L steel, alloyed with nitrogen and manganese. The additional increase of Mn and the addition of Cu result in a 5-times increase of the corrosion rate in all processing conditions. The pitting corrosion resistance of 213 L is higher than that of 212 L, perhaps because of the tungsten addition. It is notable that neutron irradiation up to $3x10^{17}$ n/cm^2 decreases the rate of corrosion in some conditions, which could be caused by radiation-induced stress relaxation [41]. Pitting corrosion was almost not observed in the 211 L and 213 L steels after annealing for 30 min at 1050°C and neutron irradiation to $3x10^{17}$ n/cm^2.

3.4 Effect of sensitization and neutron irradiation on pitting corrosion resistance of 316 LN steel alloyed by nitrogen, manganese, copper and tungsten.

The effect of the aging temperature on the corrosion rates of as-cast and cold-rolled 316 LN steel, both irradiated and unirradiated, is shown in Figure 5.

Commented [MPS5]: Error bars? How would they be calculated? Also, please show the Treatment Number from Figure 1 that these correspond to.

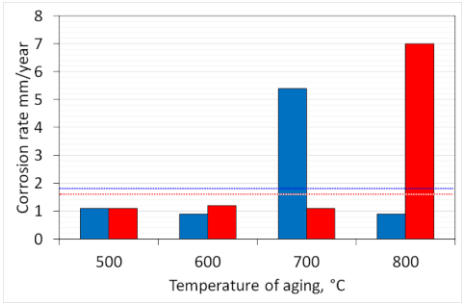

a b

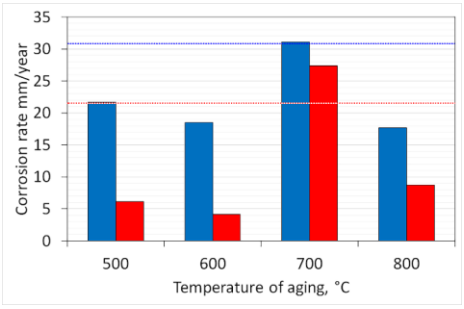

Figure 5: Corrosion rate values of as-cast (a) and cold-rolled (b) 316 LN steel after thermal aging, unirradiated (blue) and irradiated to $3x10^{17}$ n/cm^2 (red). For comparison, the corrosion rates of unaged samples was added from Figure 4 as dotted blue and red lines for the unirradiated and irradiated conditions, respectively.

After thermal treatment in the 500 – 600°C range for 1 hour, the resistance to pitting corrosion of 316 LN steel increases due to stress relaxation processes [42]. At these temperatures, sensitization, while thermodynamically possible, is kinetically limited to rates too slow to noticeably sensitize the materials. Heating at 700-800°C leads to an increase of the corrosion rate in the cast and cold-rolled 316 LN steel, because of the intensive formation of carbides and nitrides (type $Cr_{23}C_6$ or Cr_2N respectively) that begins at this temperature [7, 43].

The effect of thermal aging temperature on the corrosion rates of as-cast and cold-rolled 211-213L steels is shown in Figure 6. Surface microstructures of the 212 L variant subject to different aging and irradiation conditions are shown in Figure 7.

Commented [MPS6]: Why are microstructures of only 212 L shown here? The reader will want to see the others.

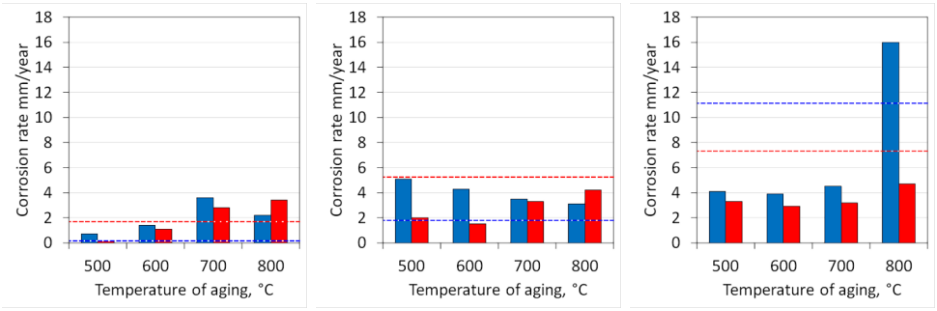

a b c

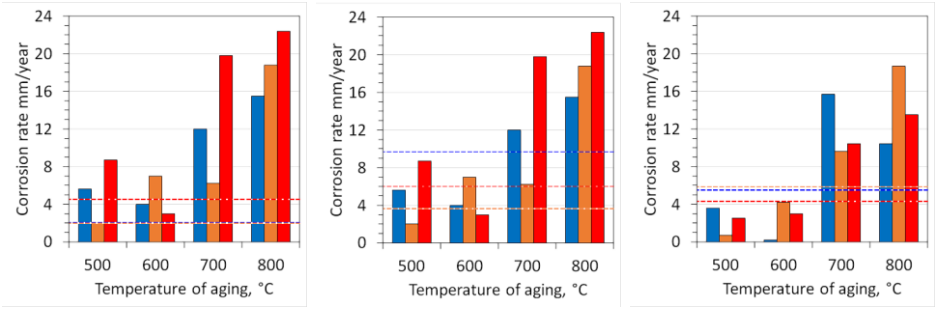

d e f

Figure 6: Corrosion rates of cast (a, b, c) and cold-rolled (d, e, f) 211 L (a, d), 212 L (b, e), 213 L (c, f) stainless steels after thermal aging. Conditions: unirradiated (blue) and irradiated to $1x10^{17}$ n/cm^2 (orange) and $3x10^{17}$ n/cm^2 (red). For comparison, corrosion rate data of unaged samples was added from Figure 4 as dotted lines.

Commented [MPS7]: Error bars? How many measurements taken in each case, and what was the uncertainty in each measurement?

Commented [MPS8]: Suggest to label the graphs directly with the conditions and alloy variant, for much easier readability.

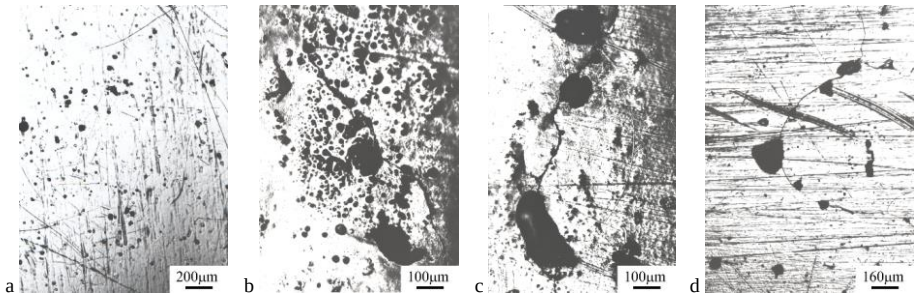

a b c d

Figure 7: Pits on the surface of cast 212 L after immersion for 72 h in 10% $FeCl_3 \cdot 6H_2O$: homogeneous distribution (a); accumulation of pits in an area with chemical structural irregularity (b); pits which have nucleated on and near grain boundaries in unirradiated steel (c) and after 1 h aging at 600°C and irradiation to $3x10^{17}$ n/cm^2 (d).

Superficial attack with no deep pits was observed in the as-cast steels. The distribution of pits was observed to be homogeneous over the sample surface (Figure 7a). More pitting was observed in areas with elemental inhomogeneity (Figure 7b). It was earlier shown that MnS particles might exist in the modified cast steels, both on grain boundaries and in the matrix [23]. These particles could be places of preferential origin of pits. On and near the grain boundaries the depth of pits was 0.3 - 0.4 mm (Figure 7c), associated with a relatively low corrosion rate. It should be noted that intergranular corrosion does not appear in the modified cast unaged steels. However, aging for one hour at temperatures above 600°C leads to grain boundary corrosion.

Commented [MPS9]: This needs a cross-sectional micrograph, unless you are assuming that they are spherical.

The level of internal stresses is known to be much lower in as-cast steel than in cold-rolled steel. Therefore, an improvement of corrosion resistance after heat treatment was not observed for the as-cast steels (Figure 6a-c). During heating, the formation of carbides and chromium nitrides occurs predominantly along the grain boundaries, which subsequently serve as centers for pitting initiation. As a result, many large pits (deepest depth ~0.5 - 0.6 mm) located along the grain boundaries (Figure 7d) were observed in the investigated steels.

Irradiation with neutrons decreases the corrosion resistance of as-cast steel, probably due to the formation of point defects and defect clusters. These can act as nucleation sites for pits to form, should they exist on or near the material surface. Some improvement in corrosion properties was observed after irradiation of the aged samples. The corrosion rate increased predictably in cold-rolled 211-213L steels after heating at 700 – 800°C. The corrosion rate then decreases slightly in cold-rolled steels after irradiation with neutrons, possibly due to a stress relaxation effect from the neutron irradiation. It is known that irradiation can relax stresses induced by significant cold-rolling above 20% in austenitic stainless steels [REF – Was book].

One significant observation was that the intensity of pitting corrosion in cold-rolled steel is different for surfaces that were either perpendicular to, or parallel to, the rolling plane (Figures 8a-b). This anisotropy arises as a result of

rolling in the production of steel. The corrosion damage observed on the planes along the rolling direction is much less than those across the rolling direction. Relatively weak corrosion of grain boundaries was detected on the planes across the rolling direction.

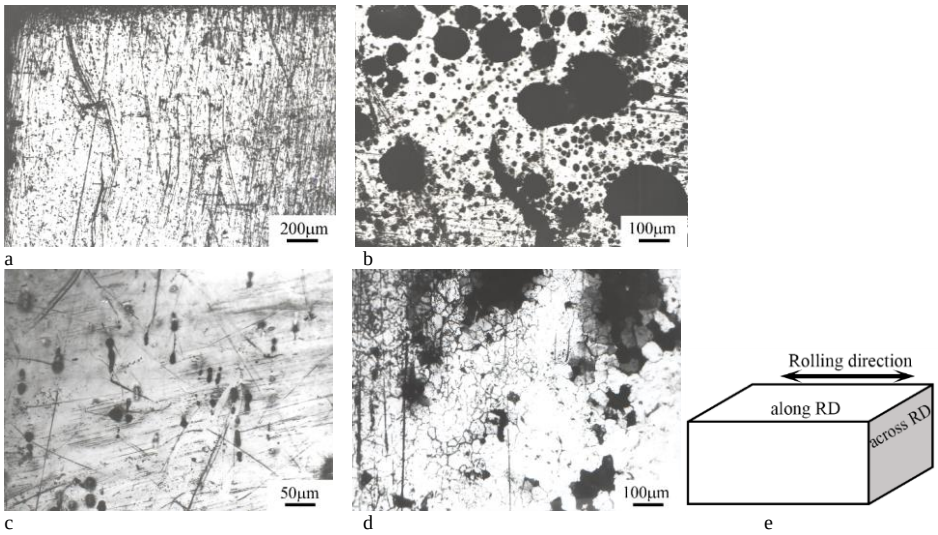

Figure 8: Optical micrographs of the surface after immersion for 72 h in 10% $FeCl_3 \cdot 6H_2O$: cold-rolled 316 LN (a, b) and 213 L steels with GBE (c, d) along (a,c) and across (b, d) the rolling direction as showed on a diagram of the sample (e).

In the modified cold-rolled and GBE-processed specimens, a strong anisotropy of the corrosion resistance was observed. According to [44], plastic deformation changes grain size and crystalline orientation during manufacturing of stainless steels. Localized zones appear and generate residual stresses in the material and as a result, anisotropy of stress and structure appear. Microstructural differences cause the differences in mechanical properties [45] and corrosion resistance [46]. The direction of rolling mainly develops the most pitting corrosion (Figures 8a, 8c).

The corrosion damage on the planes parallel to the rolling direction was very similar for both cold-rolled and GBE steels – small, shallow pits. Nevertheless, on the planes which were perpendicular to the rolling direction, another behavior was observed. In the cold-rolled steels, relatively large pits were detected (Figure 8a), while in the GBE steel, intergranular attack is quite prevalent (Figure 8d). Grain boundary attack via intergranular corrosion leads to grains dropping out of the metal surface in some areas. In GBE alloys, pits formed with a depth of ~0.2 mm, while in the cold-rolled alloys depths ranged from 0.2 to 0.6 mm.

3.5 Pitting and corrosion resistance of the steels after GBE

The effect of neutron irradiation on the corrosion rate of GBE-treated stainless steels is shown in Table 3. In the GBE materials, as in the case of the as-cast and cold-rolled materials, alloying with copper led to a significant deterioration in corrosion resistance. The corrosion rates of 211 L samples are several times lower than those of 212 L and 213 L, which contain significantly more copper. Neutron irradiation up to a maximum fluence of $3 \cdot 10^{17}$ n/cm^2 leads to an improvement in corrosion resistance of these steels after GBE treatment. A significant decrease in corrosion rate was observed in the 211 L steel, both in an absolute sense and following irradiation.

Table 3: Corrosion rates (mm/year) of 211- 213 L stainless steels after GBE

	Fluence (n/cm^2)		
Material	Unirradiated	1.3×10^{17}	3.2×10^{17}

Commented [MPS10]: I thought your fluences only went up to 3×10^{17}

211 L	0.9	0.3	0.3
212 L	6.5	3.7	5.7
213 L	2.6	1.9	2.8

The effects of thermal aging and subsequent neutron irradiation on the corrosion rate of modified 316LN variants is shown in Table 4. Aging at 700°C of steels with GBE treatment leads to a sudden increase in corrosion rate by 4 - 5 times for unirradiated 211 L and 212 L steels. As a result of neutron irradiation up to $2.7 \cdot 10^{17}$ n/cm^2, the resistance to pitting corrosion increased significantly. The corrosion rate of cold-rolled steels after annealing at 1050°C for 30 min was comparable to steels after GBE.

Table 4: Corrosion rates (mm/year) of the thermally aged (sensitized) 211- 213 L variants after GBE

Material	500°C, 1h	600°C, 1h	700°C, 1h
unirradiated			
211 L	0.2	1.0	6.1
212 L	8.0	7.1	24.3
213 L	1.8	5.7	5.1
$2.7 \cdot 10^{17}$ n/cm^2			
211 L	0.1	1.0	1.9
212 L	3.1	3.0	6.8
213 L	2.2	1.0	3.7

Conclusions

1. The effects of neutron irradiation, thermo-mechanical treatment, sensitization temperature, and compositional variation on the susceptibility of 316LN stainless steel to pitting corrosion were investigated. Neutron irradiation to $3 \cdot 10^{17}$ n/cm^2 (E > 1.1 MeV) either does not affect or sometimes slightly improves the resistance to pitting corrosion in modified 316 LN variants. Aging at low temperature (500-600°C for 1 hour) slightly improves the corrosion properties due to relaxation of internal stresses, although at an aging temperature of 700°C sensitization occurs with a sudden increase of the corrosion rate in cold-rolled and GBE-treated steels. The GBE treatment significantly improves plasticity and resistance to pitting corrosion compared to the cold-rolled condition.

Pitting tests of 316 LN-based steels alloyed with nitrogen, manganese, copper, and tungsten confirmed that the modified steels usually significantly exceed the corrosion resistance of the unmodified 316LN steel. The best localized corrosion resistance is shown by the steel variant alloyed with nitrogen and manganese. The corrosion rate of unirradiated 211 L steel in all investigated conditions is more than 15 times lower than that of unirradiated 316 LN steel in the same conditions. Copper and tungsten reduce the resistance to pitting corrosion.

In cold-rolled and GBE steels, an anisotropy of the corrosion resistance was observed on faces parallel to or perpendicular to the rolling direction. The corrosion damage on the planes parallel to the rolling direction was very similar for both cold rolled and GBE steel. On the planes which were perpendicular to the rolling direction relatively big pits were mainly detected in cold-rolled steels, while in the steels after GBE intergranular attack is quite prevalent. Grain boundary attack via intergranular corrosion leads to grains dropped out of the metal surface in some areas. It probably occurs because of anisotropy of stress and structure developed during cold-rolling.

Commented [MPS11]: Needs one final, short paragraph. Which steel variant and conditions produces the best resistance to pitting corrosion, and why? What will be your future work?

References

[1] P. Atanda, A. Fatudimu, O. Oluwole, J. of Minerals and Materials Characterization and Engineering, Vol. 9, No.1, pp. 13-23, 2010.
[2] P. Zahumensky *et al.* Corrosion Science, Vol.41, No.1, pp.1305-1322, 1999.
[3] J. Kysela, V. Broz, J. Srank , ENS RRFM '99. Transactions
http://www.iaea.org/inis/collection/NCLCollectionStore/_Public/32/034/32034888.pdf
[4] A. Barbucci, G. Cerisola, P.L. Cabot, J Electrochem Soc., Vol.149, No.12, B534-42, 2002.
[5] H. Krawiec *et al.*, Metallurgical and Materials Transactions A, Vol. 35, No.11, pp.3515-21, 2004.
[6] A. Rossi, B. Elsener, G. Hahner, M. Textor and N. D. Spencer, Surf. Interface Anal. Vol.29, pp.460–467, 2000.
[7] Hong Shih, ed., *Corrosion Resistance* (Croatia: InTech, 2012, ISBN 978-953-51-0467-4).
[8] U.K. Mudali, *et al.* Corrosion Science, Vol. 44, No.10, pp.2183-2189, 2002.
[9] M.O. Speidel, Mat-wiss. u. Werkstoiftech., Vol.37, No.10 pp.875-880, 2006.
[10] X. P. Ma, L.J. Wang, B. Qin, C.M. Liu, S.V. Subramanian, Materials and Design, Vol.34, pp.74–81, 2012.
[11] Q. Ran, Y. Xu, J. Li, J. Wan, X. Xiao, H. Yu, L. Jiang, Materials and Design, Vol.56, pp.959–965, 2014.
[12] T. Tsuchiyama, H. Takebe, K. Tsuboi and S. Takaki, Scripta Materialia, Vol. 62, pp.731–734, 2010.
[13] I. LeMay and L.M. Schetky, *Copper in Iron and Steel* (New York, NY: John Wiley and Sons Inc., 1982).
[14] B.M. Gonza ´lez, *et al.* Mater. Sci. Eng. A, Vol.343, pp. 51-56, 2003.
[15] H. Geng *et al.*, J. Mater Sci., Vol.43, No.1, pp.83-72, 2008.
[16] T. Sourisseau, E. Chauveau, B. Baroux, Corrosion Science, Vol. 47, No.5, pp.1097-117, 2005.
[17] H.T. Lin, W.T. Tsai, J.T. Lee, C.S. Huang, Corrosion Science, Vol. 33, pp.691-697, 1992.
[18] H. Ohashi, T. Adachi, K. Maekita, Tetsu to Hagane Vol.66, p.1309, 1980.
[19] A. Pardo, M.C. Merino, M. Carboneras, A.E. Coy, R. Arrabal, Corrosion Science, Vol. 49, pp.510–525, 2007.
[20] A.A. Hermas, I.M. Hassab-Allah, J. Materials Science, Vol. 36, No. 14, pp.3415-22, 2001.
[21] B. Wallen, M. Liljas, and P Stenvall, Materials and Design, Vol.13, pp.329–333, 1992.
[22] G. Rondelli, B. Vicentini, A. Cigada Materials Corrosion, Vol.46, No.11, pp.628-32, 1995.
[23] E.A. Kenik, *et al.*, Journal of Nuclear Materials, Vol.483, pp.35-43, 2017.
[24] K.T. Slattery, D.E. Driemeyer, Cassette Body Cast/HIP Development, ITER Technical Note, ITER/US/98/IV-DV-09, 1998.
[25] E.A. Trillo, L.E. Murr, J. J Materials Science, Vol. 33, No.5, pp.1263-1271, 1998.
[26] J. T. Busby, *et al*. Improved Cast Stainless Steels for ITER Shield Modules; 2008 Annual Report, ORNL/TM-2008/175, Sept. 2008.
[27] R. Jones, V. Randle, Mat.Sci.Eng. Vol. A527, pp.4275-4280, 2010.
[28] L. Tan, T. R. Allen, and J. T. Busby, Journal of Nuclear Materials, Vol.441, pp.661–666, 2013.
[29] T. Watanabe, Journal of Materials Science, Vol.46, pp. 4095–4115, 2011.
[30] V. Randle, Materials Science and Technology, Vol. 26, No.3, pp.253-261, 2010.
[31] J. T. Busby, *et al.* Journal of Nuclear Materials, Vol.417, pp. 866–69, 2011.
[32] A.H. Bott. F.B. Pickering, G.J. Butterworth, Journal of Nuclear Materials, Vol.141-143, pp. 1088-1096, 1986.
[33] M. Nystrom, U. Lindstedt, B. Karlsson, and J.-O. Nilsson, Materials Science and Technology, Vol.13, pp.560–567, 1997.
[34] J.Y. Jonsson, L. Wegrelius, S. Heino, M. Liljas, R. Ostberg, Materials Science Forum, 318–320, 511–516, 1999.
[35] K. M. Kim and K. Y. Kim, Journal of Power Sources, Vol. 173, 917–924, 2007.
[36] N. Tricot, U. Jendrich, Neutron fluence at the reactor pressure vessel wall a comparison of french and german procedures and strategies in PWRs. – Institut de Radioprotection et de Surete Nucleaire, 2003. – №. IRSN-DES--546.
[37] ASTM G 48-03, Standard Test Methods for Pitting and Crevice Corrosion Resistance of Stainless Steels and Related Alloys by Use of Ferric Chloride Solution, 2003.
[38] Byun TS, Farrell K. Plastic instability in polycrystalline metals after low temperature irradiation. Acta Materialia. 2004 Apr 5;52(6):1597-608.
[39] S.-X. Li, *et al*., Corrosion Science, Vol. 66, pp.211–216, 2013.
[40] M. Beckert und H. Klemm. *Handbuch der metallographischen Ätzverfahren* (Aufl. VEB Deutscher Verlag für Grundstoffindustrie, Leipzig-Ln, 1976), 410.

Commented [MPS12]: ???

[41] Kaji Y. et al. Development of damage evaluation method considering radiation induced stress relaxation. – 2007. – №. IAEA-CN--155.

[42] H. Pommier, E. Busso, T. Morgeneyer, A. Pineau, Acta Materialia, Vol.103, pp.893-908, 2016.

[43] L.J. Wang, , L.Y. Sheng, C.M. Hong, Materials and Design, Vol. 37, pp.349–355, 2012.

[44] Segura A. *et al*., NDT. net., Vol. 5, 2009.

[45] Handbook of stainless steel, Outokumpu Oyj, Finland, 92p., 2013.

[46] G. O. H.Whillock, B. F. Dunnett, M. Takeuchi, Corrosion, Vol.61, No1, pp. 58-67, 2005.